JPE 6-4-1

An Adaptive Dead-time Compensation Strategy for a Permanent Magnet Synchronous Motor Drive Using Neural Network

Naomitsu Urasaki[†*], Tomonobu Senjyu[*], Toshihisa Funabashi[**] and Hideomi Sekine[***]

[†*]Dept. of Electrical and Electronics Eng., University of the Ryukyus, Okinawa, Japan
[**]Meidensha Corporation, Tokyo, Japan
[***]Dept. of Technology Education, University of the Ryukyus, Okinawa, Japan

ABSTRACT

This paper presents a neural network based adaptive dead-time compensation strategy for an inverter fed permanent magnet synchronous motor drive. The neural network is used for identifying the dead-time compensation time (DTCT) that includes an equivalent dead-time, turn-on/off time and on-state voltage components of the voltage source inverter. In order to train the neural network, desired DTCTs for eight operating points are prepared as training data. The trained neural network can identify a desired DTCT for any operating point because it has the capability of the interpolation. The accuracy of the identified DTCT is experimentally confirmed by comparing the calculated active power with a measured one.

Keywords: dead-time, voltage source inverter, permanent magnet synchronous motor, neural network

1. Introduction

Inverter fed permanent magnet synchronous motor (PMSM) drives have widely been developed during the last decade. Several applications, such as rotor position sensorless drives and direct torque control drives, need fundamental armature voltage to calculate the armature flux linkage [1]. Since the fundamental component of the actual voltage cannot be detected directly from the inverter output terminal, commanded voltage is usually used instead of the actual one. However, commanded voltage never agrees with the fundamental actual voltage due to the nonideal characteristics of the voltage source inverter (VSI), such as dead-time, turn-on/off time of switching devices, and on-voltages of the switching devices and diodes. Dead-time is vital to avoid short-circuiting the inverter legs. Turn-on/off time and on-voltages inevitably exist in actual devices. To cope with this problem, several authors have made attempts to compensate for nonideal inverter effects [2-6]. In [2], a dead-time compensation voltage (DTCV) was introduced. The DTCV is determined from the analytical results of the average error between ideal and actual inverter output voltages. Since this method requires only dead-time and DC-link voltage, implementation is easy. However, turn-on/off time and on-voltages effects cannot be compensated. In [3], a dead-time compensation time (DTCT) was introduced instead of dead-time. The DTCT

Manuscript received March. 7, 2005; revised June. 17, 2006
[†]Corresponding Author: urasaki@tec.u-ryukyu.ac.jp
Tel: +81-98-895-8710, Fax: +81-98-895-8708, Ryukyus Univ.
[*]Dept. of Electrical and Electronics Eng., Univ. of the Ryukyus
[**]Meidensha Corporation, Tokyo, Japan
[***]Dept. of Technology Education, University of the Ryukyus

equivalently includes turn-on/off time and on-voltage components as well as dead-time. Thus, this method can compensate for not only dead-time effect but also turn-on/off time and on-voltage effects. Since DTCT is usually an unknown parameter, it should be identified. In [3], DTCT is identified with a developed adaptive identification process in advance. Then, a fixed DTCT is utilized for the dead-time compensation strategy. However, the fixed DTCT is not always valid since DTCT can vary with the operating points. For this reason, adaptive dead-time compensation strategies have been reported [7-9]. In [7], the magnitude of DTCV is adopted according to the peak value of the phase current. This method requires a number of data to prepare a look-up table. Although the method developed in [8] operates without preparing a look-up table, it requires accurate motor parameters. The strategy presented in [9] has trouble with convergence.

This paper presents a neural network based adaptive dead-time compensation strategy for a VSI fed PMSM drive. The neural network is used for identifying the desired DTCT for any operating point. In order to train the neural network, the desired DTCTs for eight operating points, i.e., eight pairs of rotor speed and armature current data, are prepared as training data in advance. The trained neural network can identify the desired DTCT for any operating point because it has the capability of interpolation. The use of neural network has the advantage that the characteristic of the desired DTCT can be identified with less data. In order to quantitatively evaluate the accuracy of the identified DTCT, the active power calculated with the use of the commanded voltage is experimentally compared with the actual active power.

2. Dead-time Compensation

2.1 Formulation of Dead-time Compensation Time

Fig. 1(a) shows the channel flow of *a*-phase current in positive direction ($i_a > 0$). The *a*-phase current i_a flows through switching device S_a^+ during the on period of S_a^+. Conversely, it flows through diode D_a^- during both the off period of S_a^+ and dead-time period. Thus, the *a*-phase inverter output voltage v_a for the dead-time period is equal to that for off period S_a+. The relationship between the a-phase ideal and actual inverter output voltages for $i_a > 0$ is shown in Fig 1(b). Due to dead-time T_d, the actual voltage becomes v_a^{dt}. Additionally, due to the turn-on time t_{on} and turn-off time t_{off} of switching device S_a^+, actual voltage becomes $v_a^{dt/tn}$.

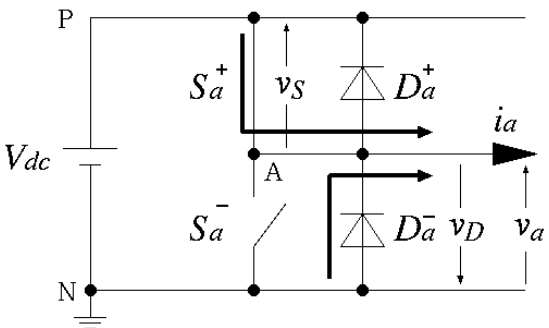

(a) Channel flow of a-phase current

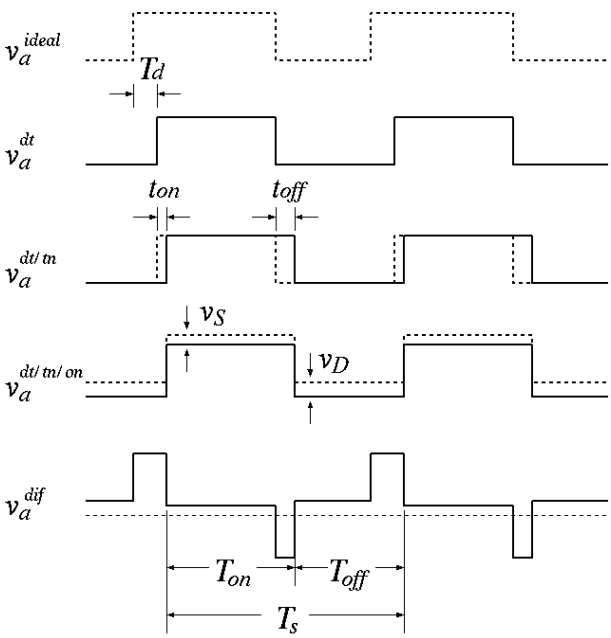

(b) a-phase inverter output voltage waveform

Fig. 1 Relationship between a-phase ideal and actual inverter output voltages for ia > 0

Furthermore, due to the on-voltages v_S of switching device S_a^+ and v_D of diode D_a^-, the actual voltage becomes $v_a^{dt/tn/on}$. As a result, the difference between the ideal and actual inverter output voltages becomes v_a^{dif} ($=v_a^{ideal} - v_a^{dt/tn/on}$).

Fig. 2(a) shows the channel flow of *a*-phase current in negative direction ($i_a < 0$). The *a*-phase armature current i_a flows through diode D_a^+ during both the on-period of S_a^+ and dead-time period. Conversely, it flows through switching device S_a^- during the off period of S_a^+. Thus, *a*-phase inverter output voltage v_a for dead-time period is equal to that for the on period of S_a^+. The relationship

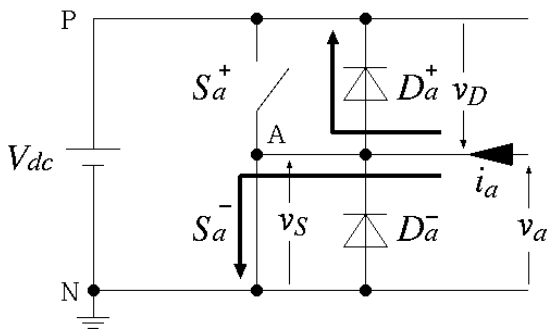

(a) Channel flow of *a*-phase current

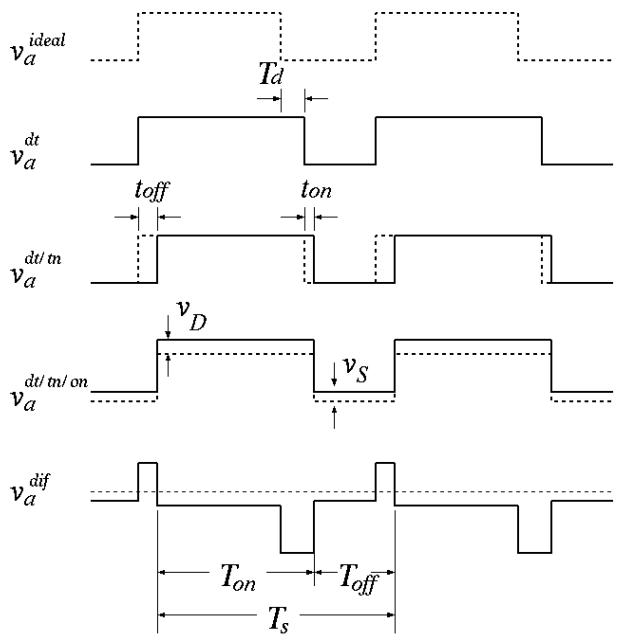

(b) *a*-phase inverter output voltage waveform

Fig. 2 Relationship between *a*-phase ideal and actual inverter output voltages for $i_a < 0$

between a-phase ideal and actual inverter output voltages for $i_a < 0$ is shown in Fig 2(b). From a similar analysis, the difference between the ideal and actual inverter output voltages becomes v_a^{dif} (= $v_a^{ideal} - v_a^{dt/tn/on}$).

To compensate for nonideal inverter effects due to dead-time, turn-on/off time, and on-voltages, an average value of the difference v_a^{dif} between the ideal and actual inverter output voltages over switching period T_s should be added to the commanded voltage of the vector controlled PMSM drive system as a DTCV. Since the magnitude of the average values of difference v_a^{dif} for both the current directions are the same and the signs are opposites, *a*-phase DTCV v_a^{com} is derived as

$$v_a^{com} = \frac{T_c}{T_s} V_{dc} \operatorname{sgn}(i_a) \tag{1}$$

where T_c, T_s, and V_{dc} are DTCT, switching period, and DC -link voltage, respectively. DTCT is defined as

$$T_c = T_d + t_{on} - t_{off} + \frac{V_{dev}}{V_{dc}} T_s \tag{2}$$

where T_d, t_{on}, t_{off}, and V_{dev} respectively are dead-time, turn-on time, turn-off time, and average on-voltage. The average on-voltage V_{dev} is defined as

$$\left.\begin{aligned} V_{dev} &= \frac{T_{on}}{T_s} v_S + \frac{T_{off}}{T_s} v_D \quad \text{for} \quad i_a > 0 \\ V_{dev} &= \frac{T_{off}}{T_s} v_S + \frac{T_{on}}{T_s} v_D \quad \text{for} \quad i_a < 0 \end{aligned}\right\} \tag{3}$$

where v_D and v_S respectively are the on-voltages of diodes and switching devices, and T_{on} and T_{off} respectively are the on period and off period of the upper-arm of the inverter legs. Fig. 3(a) shows the experimental results for the duty factor (D_f=T_{on}/(T_{on}+T_{off})) of the a-phase inverter output voltage versus the instantaneous value of the phase current for various power factors. Table 1 lists the specifications of the laboratory inverter. An insulated gate bipolar transistor (IGBT) module is utilized for the switching devices. It follows that the duty factor varies with the instantaneous value of the phase current in the region of 50%. Duty factor also depends on power factor because it relates to phase voltage rather than current. Fig. 3(b) shows the average value of the on-state voltage calculated from (3) in which the on-state voltages v_S and v_D are 1.9V and 2.5V,

respectively. As can be seen from Fig. 3(b), the average on-state voltage is not the same at positive and negative values of the phase current in a precise sense. However, the average on-state voltage is assumed to be the same irrespective of the polarity of the phase current because the difference is negligibly small (within 0.05V). This assumption is valid as long as the duty factor of the inverter output voltage remains around 50%.

2.2 Desired Dead-time Compensation Time

The proposed strategy attempts to form an agreement between the commanded voltage generated through the current controller and the fundamental component of the actual voltage by compensating for the effects of nonideal inverter characteristic such as dead-time.

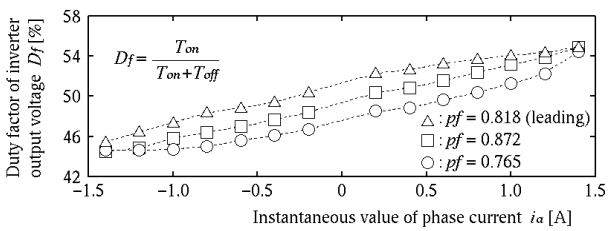

(a) Duty factor

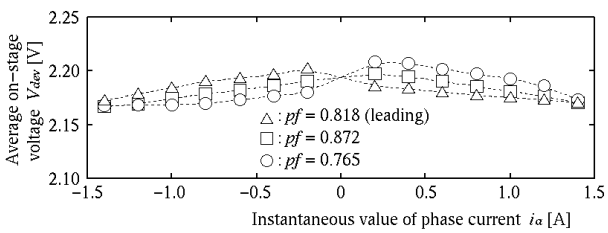

(b) Average on-state voltage

Fig. 3 Duty factor of inverter a-phase output voltage and average on-state voltage in terms of the instantaneous value of phase current for various power factors

Table 1 Specifications of laboratory inverter (IGBT module PM30CSJ060)

Maximum rated voltage	V_{ce}	600V
Maximum rated current	I_C	30A
Turn-on time	t_{on}	0.6μs
Turn-off time	t_{off}	2.0μs
On-state voltage of IGBT	v_S	1.9V
On-state voltage of diode	v_D	2.5V

A desired DTCT yields the appropriate commanded voltage which corresponds with the fundamental component of the actual voltage. Thus, it is advisable to determine the desired DTCT from a comparison between the commanded voltage and the fundamental component of the actual voltage. However, detecting the fundamental component of actual voltage is complex. Instead, active power is used for evaluating the accuracy of the DTCT. That is, the active power measured with the power meter is compared with the active power calculated from

$$P_{in} = v_d^* i_d + v_q^* i_q \tag{4}$$

where v_d^* and v_q^* are the *d-q*axes commanded voltages, i_d and i_q are the actual currents transformed into the synchronous *d-q* axes reference frame. Since the phase current for the PWM VSI has little harmonic components, measured active power also has little harmonic components even if the phase voltage has harmonic components. In contrast, if the commanded voltage has harmonic components, calculated active power is greater than the fundamental one. In other words, if the calculated power corresponds with measured one, the calculated voltage agrees with the fundamental component of the actual voltage. For this reason, the desired DTCTs for the various operating points have been determined such that the calculated active power agrees with the active power measured with the digital power meter WT230 on the typical vector controlled PMSM drive system shown in Fig. 4.

Fig. 5 shows the characteristics of the DTCT which consists of 20 plots, i.e., 4 rotor speeds (1000, 1500, 2000, and 2500 rpm) times 5 armature currents (0.5, 1.0, 1.5, 2.0, and 2.5 A). It follows that the DTCT decreases with increasing rotor speed. The authors deduce the reason for this is as follows. Desired DTCTs are determined such that the commanded voltage generated through the current controller agrees with the fundamental armature voltage. In other words, a desired DTCT relates to the degree of impact of the nonideal inverter on the current controller. Thus, a desired DTCT decreases in high-speed regions in which the impact of nonideal inverter is relatively low compared to low-speed regions.

The specification of the IGBT module indicates that

both the on-voltages v_S and v_D at high temperatures (125°C) are lower than those at low temperatures (25°C) by about 0.25V. Fig. 6 shows the variation of the desired DTCT operating times. Armature current is kept at 2.5A in this operation. Thus, the temperature of the IGBT module should increase with the operating time.

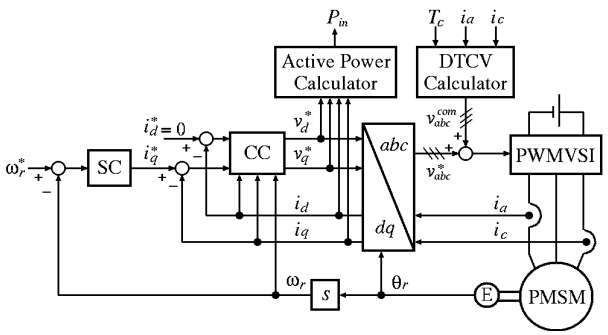

Fig. 4 Vector controlled PMSM drive system for determining desired DTCT

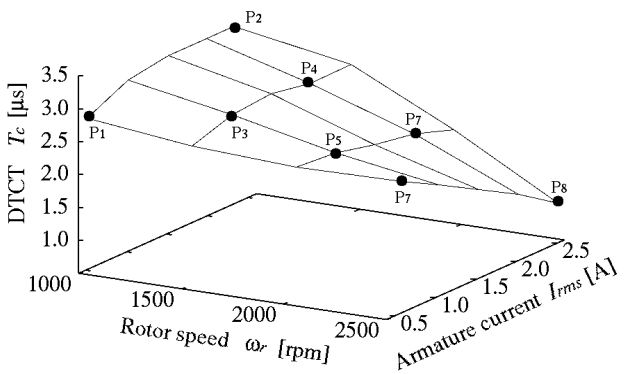

Fig. 5 Characteristic of the desired DTCTs for various operating points

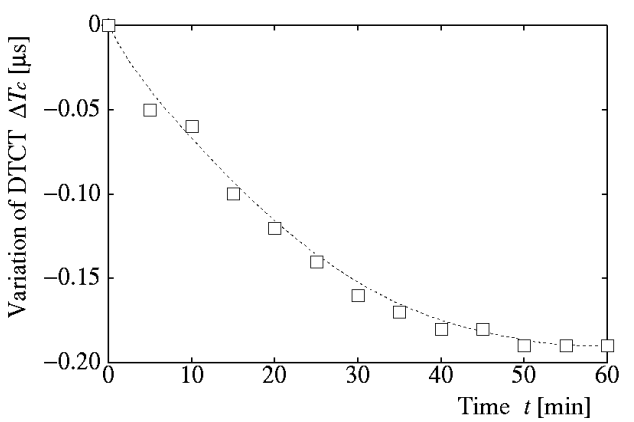

Fig. 6 Variation of DTCT for operating point under constant phase current

Although an accurate temperature of the IGBT module is not available due to the absence of a temperature sensor, the fact that the desired DTCT decreases with operating time is consistent with the decrease of on-voltages v_S and v_D. Although temperature variation is ideally considered, it in not incorporated in this strategy for the following reasons:

1. The variation of the DTCT due to temperature variation is not significant.
2. It is difficult to obtain the temperature of IGBT module on-line without a temperature sensor. In addition, the authors think that the installation of a temperature sensor is not a reasonable solution.

To adaptively change the DTCT according to the operating point, the desired DTCT should be stored in a look up table. However, it is unrealistic to experimentally determine twenty or more DTCTs in advance. To overcome this problem, a neural network is used for identifying the characteristics of the desired DTCT. Since the neural network has the capability of interpolation, it can identify the characteristics with less data. In this case, eight DTCTs, which correspond to operating points (P_1, P_2, ⋯, P_8) indicated in Fig. 5, are prepared as the training data of the neural network. In the next section, the architecture and training algorithm of the neural network are discussed in detail.

3. Dead-time Compensation Time Identification by Neural Network

3.1 Neural Network Architecture

Fig. 7 shows the architecture of the three-layer feed forward neural network for identifying the characteristics of the DTCT indicated in Fig. 5. The neural network consists of an input layer, hidden layer, and output layer. Each layer has some units that are connected to units of the upper layer with connection weights such as w_{ji} or w_{kj}. Input to a j-th unit x_j is the sum of the output units of the lower layer y_i multiplied by the connection weight w_{ji}:

$$x_j = \sum_{i=1}^{I} (w_{ji} y_i) \tag{5}$$

where I is the number of units of the lower layer. The input is transmitted to the upper layer through a nonlinear transfer function as

$$y_j = h(x_j) \tag{6}$$

The nonlinear function plays an important rule in giving the neural network a nonlinear mapping property. In this paper, the sigmoid function indicated in (7) is used as a nonlinear transfer function for the following reasons:

1. It is easy to implement the error back-propagation algorithm that will be discussed in Section 3.2.
2. The output of the sigmoid function is positive for any input signal. This is suitable for identifying the DTCT because it should be positive.

$$h(x_j) = \frac{1}{1+\exp^{-x_j}} \tag{7}$$

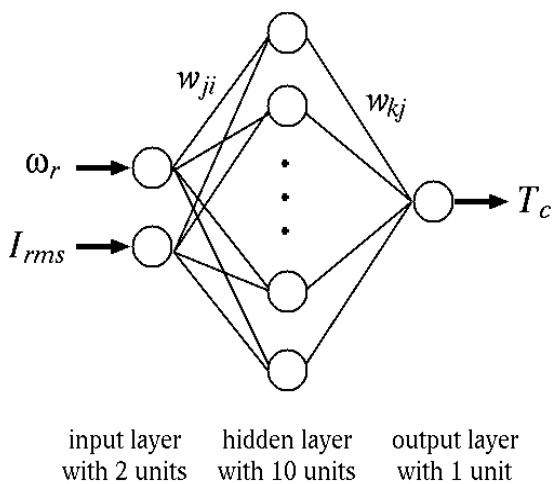

Fig. 7 Architecture of neural network

The output of the neural network is identified DTCT T_c. The input of the neural network are rotor speed ω_r and armature current I_{rms} (= $\{(i_d^2 + i_q^2)/3\}^{1/2}$) in rms value. The number of units of the hidden layer is usually determined by trial and error. The units from 1 to 30 have been tried in this research. As a result, the minimum number of units of the hidden layer, which has good identification ability, is 10. For this reason, the number of units of the hidden layer is set at 10.

3.2 Error Back-Propagation Algorithm

In order to train the neural network training data corresponding to eight operating points: P_1 (ω_r =1000rpm, I_{rms}=0.5A), P_2 (1000rpm, 2.5A), P_3 (1500rpm, 1.0A), P_4 (1500rpm, 2.0A), P_5 (2000rpm, 1.0A), P_6 (2000rpm, 2.0A), P_7 (2500rpm, 0.5A), and P_8 (2500rpm, 2.5A) indicated in Fig. 5 are prepared.

The error back-propagation algorithm (EBPA) is utilized for the training of the neural network. EBPA is based on the gradient descent method, i.e., connection weights are iteratively updated so that error function E_d can decrease:

$$w_{ji}[n+1] = w_{ji}[n] + \eta\left(\frac{\partial E_d}{\partial w_{ji}[n]}\right) + \alpha\Delta w_{ji}[n] \tag{8}$$

where $\Delta w_{ji} = w_{ji}[n] - w_{ji}[n-1]$, n is the number of step, η and α are training rate and momentum coefficient, respectively. The error function is defined as

$$E_d = \frac{1}{2}\sum_{k=1}^{K}(t_{dk} - o_{dk})^2 \tag{9}$$

where t_{dk}, o_{dk}, and K are desired output, the output of the neural network, and the number of units of the output layer, respectively.

Fig. 8 shows the transition of the following mean absolute error (MAE) for the training of the neural network.

$$E_{ma} = \frac{1}{DK}\left|\sum_{d=1}^{D}\left\{\sum_{k=1}^{K}(t_{dk} - o_{dk})\right\}\right| \tag{10}$$

where D is the number of training data. In this case, training rate η and momentum coefficient α are set at 0.2 and 0.5, respectively. As can be seen from Fig. 8, 100,000 times of iteration for training makes the MAE sufficiently decrease. Fig. 9 shows the desired DTCTs for the various operating points identified by the trained neural network. A comparison between Figs. 5 and 9 confirms that the trained neural network successfully identifies the characteristics of the desired DTCT for any operating point. It is noted that only eight operating points are utilized for the training of the neural network.

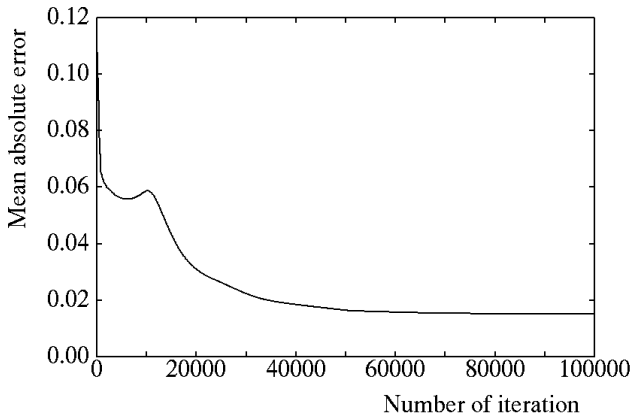

Fig. 8 Transition of mean absolute error of training

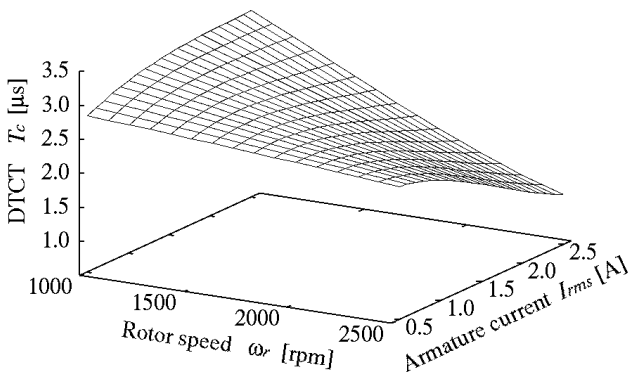

Fig. 9 Characteristic of desired DTCTs identified by the trained neural network

4. Experimental Results

Fig. 10 shows the typical vector controlled PMSM drive system with the trained neural network. PI controllers are employed in the speed controller (SC) and current controller (CC). Neural network identifies DTCT T_c from the information of the rotor speed and armature current in rms value, adaptively. Rotor speed and armature current are detected by the rotary encoder and current sensor through a 12 bit AD converter, respectively. It is noted that the rms value of the armature current is calculated from only q-axis current i_q because d-axis current i_d is zero in this system. The output of the neural network, i.e., DTCT, is updated every 800μs. The a-phase DTCV v_a^{com} is calculated from (1). The b-phase and c-phase DTCVs (v_b^{com}, v_c^{com}) are also calculated in a similar way. These DTCVs are added to commanded voltages (v_a^*, v_b^*, v_c^*). PI controllers and a neural network based dead-time compensator are implemented in DSP TMS320C32. Electrical power applied to the tested PMSM is supplied through the VSI, in which an IGBT module is utilized for the switching device. The specifications of the tested PMSM and control parameters are listed on Tables 2 and 3, respectively.

Fig. 11 shows the experimental results for the proposed dead-time compensation strategy. The tested PMSM rotates at 1000 rpm (driving frequency is 33.3Hz). Load torque is 0.1N·m (20% of the rated torque). The d-axis current i_d is controlled at zero. In order to clarify the advantageous effects of the proposed strategy, the result of the dead-time compensation strategy, not applied to the PMSM drive system, is also plotted. Fig. 11(a) shows the DTCT identified by the neural network. Since the operating point does not change in this case, the identified DTCT is almost constant ($T_c \approx 3.0$μs). Fig. 11(b) shows a-phase current i_a. Since the current controller performs well, the distortion of the phase current hardly appears irrespective of dead-time compensation, except in extreme light load conditions. Fig. 11(c) shows a-phase DTCV v_a^{com}. The amplitude of the DTCV depends on the identified DTCT, while the sign depends on the polarity of the phase current. The a-phase commanded voltage compensating for the effects of the nonideal inverter is compared with the commanded voltage without any dead-time compensation strategy in Fig. 11(d). An unwanted excessive component due to the effect of the nonideal inverter is removed by applying the proposed

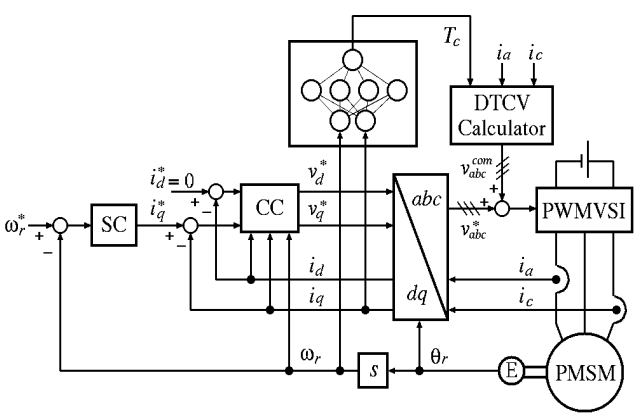

Fig. 10 Vector controlled PMSM drive system for determining desired DTCT

Table 2 Specifications of tested PMSM

Rated power	P_n	160V
Rated torque	τ_n	0.5N·m
Rated speed	N_n	3000rpm
Armature resistance	R	2.3Ω
Armature inductance	L	0.0065H
EMF constant	K_e	0.0658V·s/rad
Number of pole pairs	P	2

Table 3 Control parameters

DC-link voltage	V_{dc}	200V
Carrier frequency	f_c	5kHz
Switching period	T_s	200μs
Control period	T_{ctl}	200μs
Proportional gain for SC	K_{ps}	0.01
Integral gain for SC	K_{is}	0.30
Proportional gain for CC	K_{pc}	10
Integral gain for CC	K_{ic}	1000

dead-time compensation strategy. Note that the nonideal inverter effects commanded voltage rather than phase current on the current controlled VSI drive except in extreme light load conditions.

Although these experimental results qualitatively confirm the validity of the proposed method, it is impossible to evaluate the quantitative accuracy and the adaptation ability of the identified DTCT because commanded voltage is not compared with the fundamental component of the actual voltage. Note that detecting the fundamental component of the actual voltage on-line is complex. In order to clarify both the quantitative accuracy and adaptive ability, additional experiments have been executed.

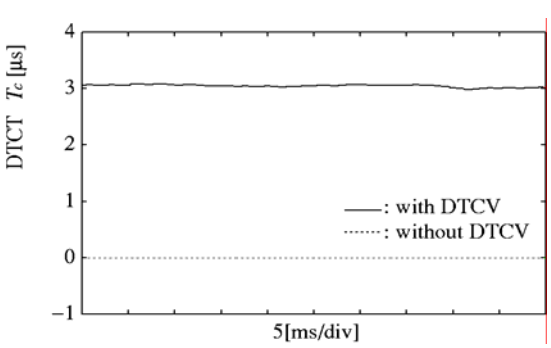

(a) Identified DTCT

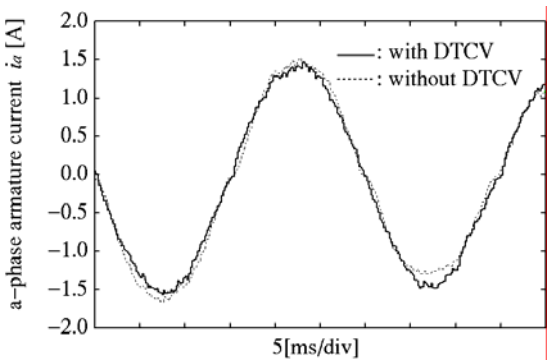

(b) *a*-phase armature current

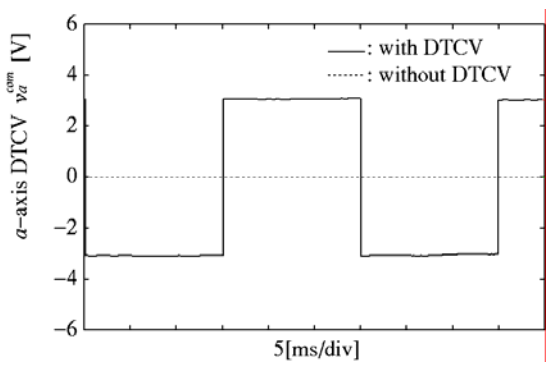

(c) *a*-phase DTCV

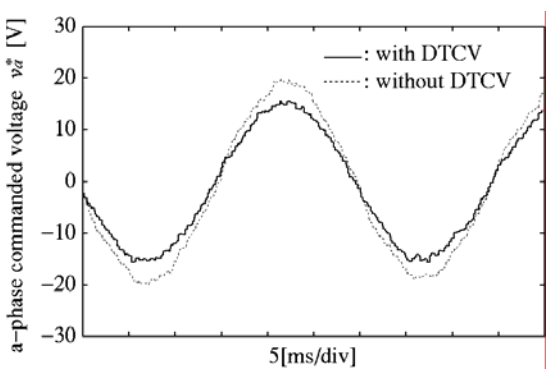

(d) *a*-phase commanded voltage

Fig. 11 Experimental results of adaptive dead-time compensation (33.3Hz (1000rpm), 1.0A)

both the quantitative accuracy and adaptation ability, additional experimentations have been executed.

Fig. 12 shows the response time of the DTCT for the step change of load torque from 0 to 0.45N·m (90% of the rated torque). Rotor speed is 2500 rpm. In order to clarify the advantageous effects of the proposed strategy, the

result for the fixed DTCT (T_c=2.8μs) is also plotted in this figure. Fig. 12(a) shows armature current I_{rms} in rms value. The armature current increases when the load torque is applied to the PMSM. As can be seen from Fig 12(b), DTCT T_c adaptively varies with the change of operating point. Fig. 12(c) shows the active power calculated with the use of the commanded voltage. Note that active power is utilized for evaluating the accuracy of the identified DTCT as explained in Section 2.2. The active power is calculated from (4). In order to quantitatively evaluate the accuracy of the identified DTCT, the measured active power for each operating point is also plotted in this figure. As compared with the fixed DTCT, the adaptive DTCT reduces the error between the measured and calculated active powers, especially in heavy load conditions.

Fig. 13 shows a comparison of results of the calculated and measured active power for various operating points to evaluate the accuracy of the identified DTCT. As can be seen from Fig. 13(a), the calculated active power without any dead-time compensation strategy disagrees with the measured one. The comparison results of the active power when the fixed DTCT (T_c=2.8μs) is applied to the dead-time compensation strategy is shown in Fig. 13(b). According to Fig. 5, the fixed DTCT is desirable for 1500 rpm. Thus, the calculated active power for 1500 rpm agrees well with the measured one. However, the calculated active power for high-speed regions above 1500 rpm is less than the measured one due to the over-setting of the DTCT. In contrast, the calculated active power for low-speed regions below 1500 rpm is greater than the measured one due to the under-setting of the DTCT. Fig. 13(c) shows the comparison results of the active power when the adaptive DTCT is applied to the dead-time compensation strategy. The calculated active power agrees well with the measured one for any operating point. These results confirm that the identified DTCT shown in Fig. 9 is valid.

Table 4 lists the mean absolute percentage error (MAPE) of calculated active power for various DTCTs.

The MAPE is defined as

$$\mathrm{MAPE} = \frac{1}{N}\sum_{n=1}^{N}\left(\frac{\left|P_{in}^{c} - P_{in}^{m}\right|}{P_{in}^{m}}\right)\times 100 \qquad (11)$$

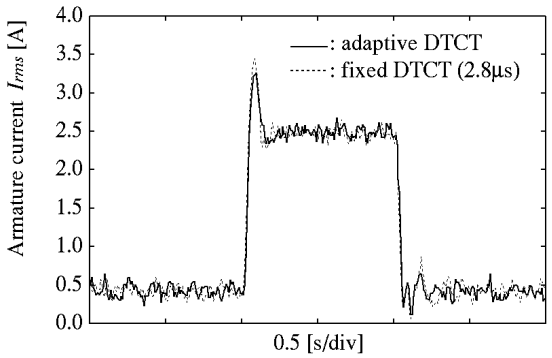

(a) Armature current

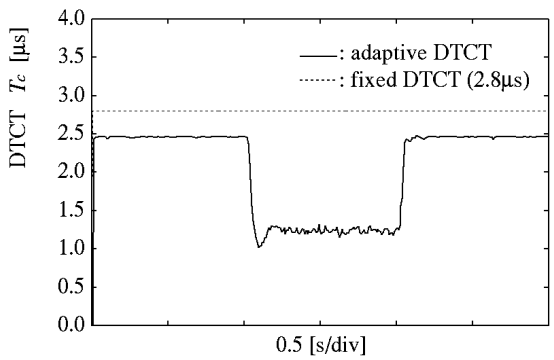

(b) Identified DTCT

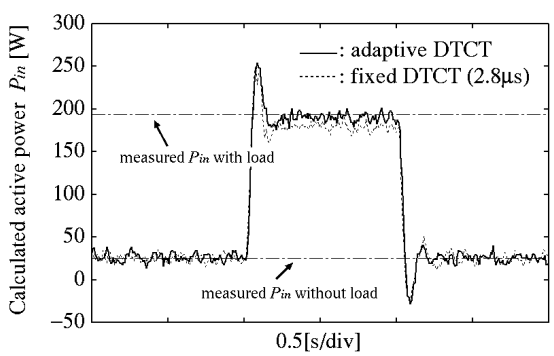

(c) Calculated active power

Fig. 12 ime response of identified DTCT for the step change of load torque

where P_{in}^{c}, P_{in}^{m}, and N denote the calculated active power, measured active power, and the number of data. As can be seen from Table 4, the MAPE for the adaptive DTCT is the smallest. This means that commanded voltage corresponds with the fundamental component of actual voltage. These experimental results confirm the usefulness of the proposed dead-time compensation strategy.

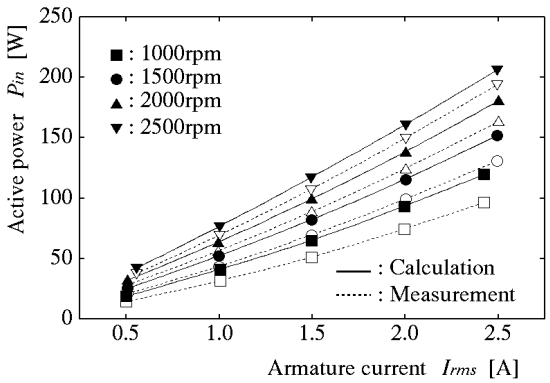

(a) Non-dead-time compensation (T_c=0μs)

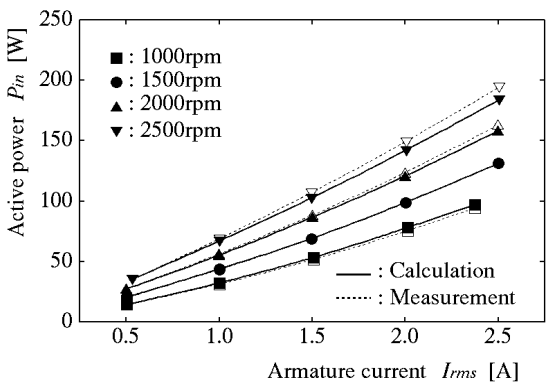

(b) Dead-time compensation with the fixed DTCT (T_c=2.8μs)

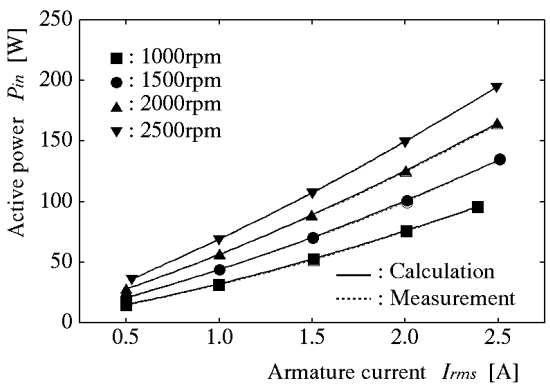

(c) Dead-time compensation with the adaptive DTCT

Fig. 13 Comparison between calculated and measured active power for various operating points

Table 4 MAPE between calculated and actual active power

Case	MAPE [%]
Non-DTCT (T_c=0μs)	16.44
Fixed DTCT (T_c=2.8μs)	2.31
Adaptive DTCT	0.75

5. Conclusions

This paper has proposed the adaptive dead-time compensation strategy for permanent magnet synchronous motor (PMSM) drive using a neural network. In the first phase, it has been pointed out that dead-time compensation time (DTCT) varies with operating points, i.e., rotor speed and load conditions. In the second phase, a neural network has been trained so as to identify a desired DTCT for any operating point. The desired DTCTs in which active power calculated with the use of commanded voltage agrees with the measured active power for eight operating points are prepared as the training data. The trained neural network can identify the desired DTCT for any operating point with less training data. Finally, the trained neural network has been incorporated in the vector controlled PMSM drive system. DTCT can quickly vary with operating point changes. Calculated and measured active powers for fixed and adaptive DTCTs are compared experimentally. The mean absolute percentage error for a fixed DTCT is 2.31%, while that for an adaptive DTCT is 0.75%. The results confirm the accuracy of the DTCT identified by a neural network and validity of the proposed dead-time compensation strategy.

References

[1] J.-S. Lee, T. Takeshita, and N. Matsui, "Stator-flux-oriented sensorless induction motor drive for optimum low-speed performance", IEEE Trans. Ind. Appl., vol. 33, no. 5, pp. 1170~1176, 1997.

[2] S.-G. Jeong and M.-H. Park, "The analysis and compensation of dead-time effects in PWM inverters", IEEE Trans. Ind. Elec., vol. 38, no. 2, pp. 108~114, 1991.

[3] J.-W. Choi and S.-K. Sul, "Inverter output voltage synthesis using novel dead-time compensation", IEEE Trans. Power Elec., vol. 11, no. 2, pp. 221~227, 1996.

[4] T. Sukegawa, K. Kamiyama, K. Mizuno, T. Matsui, and T. Okuyama, "Fully digital, vector-controlled PWM VSI-fed ac drives with an inverter dead-time compensation strategy", IEEE Trans. Ind. Appl., vol. 27, no. 3, pp. 552~559, 1991.

[5] D. Leggate and R. J. Kerkman, "Pulse-based dead-time compensator for PWM voltage inverter", IEEE Trans. Ind. Elec., vol. 44, no. 2, pp. 191~197, 1997.

[6] C. Attaianese and G. Tomasso, "Predictive compensation

of dead-time effects in VSI feeding induction motors", IEEE Trans. Ind. Appl., vol. 37, no. 3, pp. 856~863, 2001.

[7] A. R. Munoz and T. A. Lipo, "On-line dead-time compensation technique for open-loop PWM-VSI drives", IEEE Trans. Power Elec., vol. 14, no. 4, pp. 683~689, 1999.

[8] H.-S. Kim, H.-T. Moon, and M.-J. Youn, "On-line dead-time compensation method using disturbance observer", IEEE Trans. Power Elec., vol. 18, no. 6, pp. 1336~1345, 2003.

[9] H. Zhao, Q. M. J. Wu, and A. Kawamura, "An accurate approach of nonlinearity compensation for VSI inverter output voltage", IEEE Trans. Power Elec., vol. 19, no. 4, pp. 1029-1035, 2004.

Naomitsu Urasaki received his B.S., M.S., and Ph. D. degrees in Electrical Engineering from the University of the Ryukyus, Japan, in 1996, 1998, and 2004, respectively. Since 1998, Dr. Urasaki has been with the Department of Electrical and Electronics Engineering, Faculty of Engineering, University of the Ryukyus, where he is currently a Research Associate. His research interests are in the areas of modeling and control of AC motors. Dr. Urasaki is a Member of IEEE and IEE of Japan.

Tomonobu Senjyu received his B.S. and M.S. degrees in Electrical Engineering from the University of the Ryukyus, Okinawa, Japan, in 1986 and 1988, respectively, and the Ph.D. degree in electrical engineering from Nagoya University, Aichi, Japan, in 1994. Since 1988, he has been with the Department of Electrical and Electronics Engineering, Faculty of Engineering, University of the Ryukyus, where he is currently a professor. His research interests are in the areas of stability of AC machines, advanced control of electrical machines, and power electronics. Prof. Senjyu is a chartered engineer in the U.K., a senior member of IEEE, and a member of IET and IEE of Japan.

Toshihisa Funabashi received his B.S. degree in Electrical Engineering from Nagoya University, Aichi, Japan in 1975. He received his Ph. D. degree in Electrical Engineering from Doshisha University, Kyoto, Japan in 2000. In 1975, he joined the Meidensha Corporation, Tokyo, Japan, where he was engaged in research on power system analysis and is currently a senior engineer in the Power System Engineering Division. Dr. Funabashi is a chartered engineer in the U.K., a senior member of IEEE, and a member of IET and IEE of Japan.

Hideomi Sekine completed his M.S. degree in electrical engineering from Gunma University Graduate School in 1969. He became an Asistant at the same university in same year. In 1983, he became an Associate professor in the Department of Electric and Electrical Engineering of the Faculty of Engineering of same university. He has been a Professor in Department of Technology Education of the Faculty of Education, University of the Ryukyus since 1996. He obtained a Dortorate degree from Tokyo Institute of Technology, Japan. Prof. Sekine is a Member of the IEE of Japan.